Springer

KSME

Journal of Mechanical Science and Technology 31 (2) (2017) 777~784
www.springerlink.com/content/1738-494x(Print)/1976-3824(Online)
DOI 10.1007/s12206-017-0129-x

Verification of the performance of rotatable jig for a single cantilever beam method using the finite element analysis †

Dong-Kil Shin*

School of Mechanical Engineering, Yeungnam University, Gyeongbuk 38541, Korea

(Manuscript Received June 24, 2016; Revised September 30, 2016; Accepted November 3, 2016)

Abstract

The performance of new jig for single cantilever beam test method was verified by finite element analysis. Two types of jig were designed for a small specimen that had relatively short length compared to the width of cantilever; one was simple fixed jig and the other was specially designed rotatable jig. The rotatable jig has a rotatable seesaw which adjusts the experimental misalignments between the specimen and test machine. Among the three translational and three rotational misalignments, following three important factors were considered; rotation about x-axis, rotation about z-axis, and translation in y-axis. Adhesive layer was modeled by cohesive zone element, and crack propagation behavior and the deviation of energy release rate were investigated. The fixed jig showed undesired asymmetric crack propagation and large deviation of energy release rate when it had rotational misalignment about x-axis. However, the proposed new rotatable jig showed almost symmetrical crack propagation and small deviation of energy release rate regardless of misalignments. Rotational motion of the seesaw automatically compensated the rotational misalignment of the specimen. The rotatable jig also showed relatively small deviation of energy release rate compared with the fixed jig by the rotational misalignment about the z-axis. In contrast, the rotatable jig showed deviation of energy release rate by translational misalignments in the y-axis. However, the magnitude of the deviation was very small within the controllable range of experimental misalignment. In conclusion, it was found out that the proposed jig was appropriate for the measurement of adhesion of a small specimen by single cantilever beam method.

Keywords: Adhesion; Single cantilever beam method; Finite element analysis; Cohesive zone model; Crack propagation

1. Introduction

Measurement of the adhesion of small component has been became important with decreasing form factors of components such as semiconductors, smart sensors, and microelectronic devices [1-3]. In such a small and thin component, it is difficult to measure the adhesion because it is difficult to manipulate the specimen precisely. Therefore, adhesion has usually been measured by shear mode-based test methods [4, 5]. Recently, the tensile mode of adhesion has received attention because it was found out that lots of interface debondings were induced by tensile mode force [6, 7].

A Single cantilever beam (SCB) method is one of test methods with which to measure the tensile mode adhesion. Basically, the SCB method is an extension of a double cantilever beam method [8]. This method has been widely used to measure face sheet debonding [9-11]. Viscoelastic properties of foundation had been investigated [12] and pre-cracking behaviour had been considered [13]. Chen et al. [14] showed that the SCB method could be used to measure the adhesion of underfill material in a flip chip package. In spite of these valuable results, more investigations for the SCB method are required for broad application.

One difficult problem with the SCB method is the alignment of the specimen with the test machine, especially when the width of the adhesive is very large compared to the length of the cantilever. Shin et al. proposed an improved method of measuring adhesion using a single cantilever beam method [15]. In their study, a silicon chip was attached by film adhesive. The overhang structure of the silicon was used as the cantilever beam for the SCB approach. Compared to other published methods, an interesting point of their research is that they proposed a new style of jig for the loading part that is comprised of a rotatable moving part on the main body. They reported good test results using the proposed jig. However, an important but unclear factor in Ref. [15] is the verification of the performance of the jig. For general usage of their proposed test method, the characteristics and performance of the test method needs to be verified more clearly.

In general, an experimental method needs to be robust against external perturbation. To achieve consistent test results, a crack needs to propagate independent of test conditions. It is

*Corresponding author. Tel.: +82 53 810 2457, Fax.: +82 53 810 4627
E-mail address: dkshin@yu.ac.kr
† Recommended by Associate Editor Heung Soo Kim

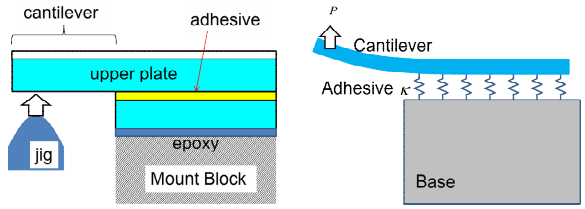

Fig. 1. Schematics of single cantilever beam test method.

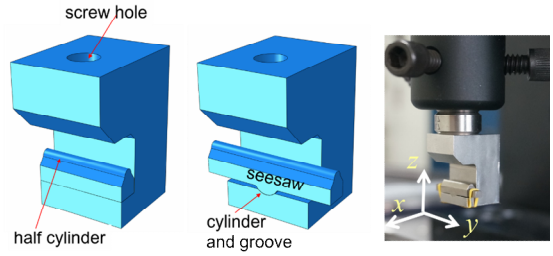

Fig. 2. Designs of jig for SCB test method: (a) Fixed jig; (b) rotatable jig; (c) photograph of rotatable jig.

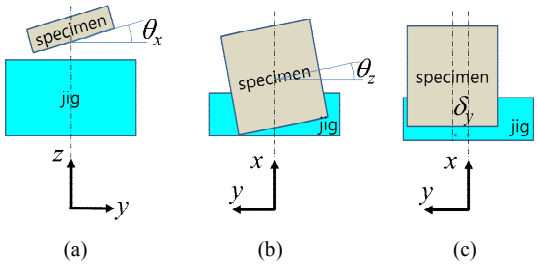

Fig. 3. Misalignments between specimen and jig: (a) Rotation about x-axis; (b) rotation about z-axis; (c) translation in y direction.

valuable to verify the behaviour of crack propagation with respect to the uncontrollable parameters of experimental conditions. Therefore, in this study, we evaluated the performance of the jig reported in Ref. [15] using numerical analysis method.

Several methods are available to simulate crack propagation. The well-known virtual crack closure technique can be used to simulate interface crack problems [16, 17]. This method is suitable for two-dimensional (2-D) or self-similar crack propagation. For general application, the Cohesive zone model (CZM) has been extensively developed for applications to delamination [18-20]. In this approach, it is assumed that there is a process zone in front of the crack tip. Damage initiates when the status of stress or strain meets certain criteria, and the damage propagates under the damage evolution law. The CZM method is an efficient method to evaluate the initiation and propagation of crack with respect to design parameters of jig and specimen.

2. Single cantilever beam method and loading jig

Single cantilever beam method is a test method to measure the adhesion using one cantilever beam. Fig. 1 shows schematics of the SCB method. A concentrated load or displacement is applied at the end of the cantilever, and a crack propagates at the interface or cohesive layer of the adhesive.

The energy release rate (G) is expressed as [8, 15]

$$G_C = \frac{P_c^2}{2b}\frac{dC}{da} \tag{1}$$

where a is crack length, b is the width of the beam, P_c is the critical load, and C is the compliance of the beam.

In this test method, an appropriate loading mechanism is required to achieve accurate test results. If the specimen is large and long enough, attaching a tab and applying a load at the tap is an efficient way to perform a test. However, if the specimen is small, it is very difficult to attach an extra assisting tab. In such a case, the loading jig must be carefully designed to ensure the accuracy of the test.

In this study, the size of the specimen is 9.6 mm x 15.2 mm with a 0.55 mm thickness. The bonding area of the film adhesive is 9.6 mm x 9.6 mm. The length of the cantilever is 2.8 mm. The thickness of the adhesive is 0.02 mm.

Fig. 2 shows two proposed types of loading jig. Each jig has a female screw (the circular hole on the upper surface) and is connected to the loading rod of the main tester. The length and width of the jig body is adjusted for the test specimen. The size of the jig is 12.0 mm wide, 16.0 mm long and 20.0 mm high. Fig. 2(a) shows a body-fixed jig. A half-cylinder is located on the L-shaped arm, and it contacts the bottom of the cantilever specimen in a straight line. As shown in the figure, it is relatively simple, and the stiffness of the jig is high enough to ensure machine rigidity. However, the fixed jig has a critical problem as indicated in Ref. [15]. With the fixed jig, it is difficult to adjust the rotational misalignment of the specimen, which is an uncontrollable parameter during specimen fabrication or in the mounting process on the test machine.

Fig. 2(b) shows a rotatable jig with a two-body structure. The contacting part with the specimen is separated from the main body. At the lower center of the separated part, there is a pair of cylinder and groove (radius is 1.8 mm). As a result, the separated part can rotate freely. The behavior of the moving part looks like a seesaw. This seesaw motion is expected to compensate the initial misalignment of the specimen automatically with a minimum loss of stiffness. From the experimental results in Ref. [15], the rotatable jig shows very good performance with a small deviation of experimental data.

Fig. 2(c) is photograph of the constructed rotatable jig connected to the loading rod. A coordinate system is also shown in the figure. The x-axis is parallel to neutral line of the cantilever beam. The z -axis is the loading direction.

There are six types of misalignments: Three translations and three rotations. The rotation about y-axis is automatically compensated by rounded shape of half cylinder of jig. The translation in x-axis is absorbed in the compliance of cantile-

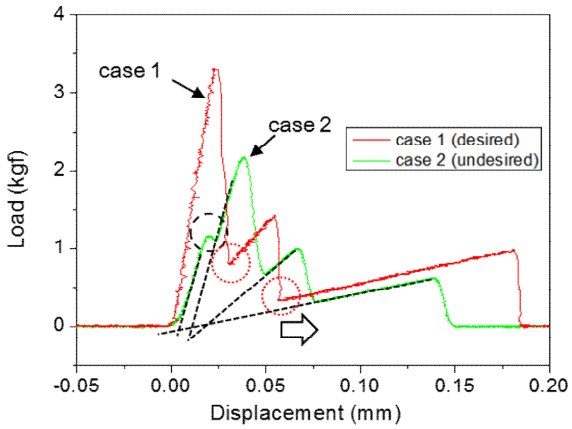

Fig. 4. Examples of load-displacement curves by single cantilever beam method.

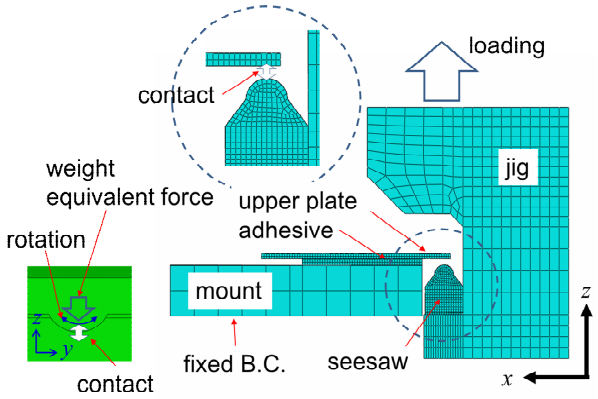

Fig. 5. Finite element model of single cantilever beam method.

ver beam. The translation in z-axis is included in loading displacement. Therefore, above three misalignments make no effect on test results. However, the other three misalignments need to be considered carefully. Fig. 3 shows definition of misalignment considered in this study: (a) Rotation about x-axis, (b) rotation about z-axis, and (c) translation in y direction.

Typical examples of the effect of misalignment are shown in Fig. 4. Case 1 shows a desired load-displacement curve which has three times of load drops by propagation of delamination. Adhesion data can be achieved at the crack arrested positions (dotted red circles). Case 2 shows small load drops at the displacement of about 0.02 mm (dashed black circle), which is resulted from the stress concentration at the corner by rotational misalignment about x-axis. And it shows much small stiffness (slope of the curve) than case 1 at the beginning of loading stage. In addition, slopes of linearly loaded segments (dashed lines) do not meets together at one point, which means it has different crack tip conditions (i.e. shape) depending on crack length.

3. Finite element modeling

The jig should make the crack propagate consistently. It is postulated that the consistency of the crack can be verified by observing the shape of the crack front as a function of the variation in specimen alignment. To verify this, a Finite element analysis (FEA) model was developed to simulate the behavior of crack propagation. The performance of the jigs was evaluated by using the commercial FEA software Abaqus/standard (Dassault systemes). Three dimensional (3-D) analysis was performed, and crack propagation was modeled by using the cohesive zone model. The effects of misalignment between the specimen and loading jig were studied parametrically.

3.1 Modeling of the jig

Fig. 5 shows the finite element model of the jig and specimen. The main body and seesaw are modeled using 3-D hexahedral continuum solid elements with eight nodes (C3D8R). The specimen and mounting jig are also modeled with solid elements. The parameter considered in this study is the delamination of the adhesive between the upper plate and lower plate. Therefore, a cohesive zone model with a traction separation law was applied at the adhesion layer. The crack propagation is simulated by using a cohesive zone model with 3-D cohesive elements (COH3D8). Detailed descriptions about the CZM are summarized in Sec. 3.2. The total number of elements is 62188, including 2880 cohesive elements. The mesh size of the adhesive layer is 0.2 mm x 0.2 mm in the xy-plane. There are two contact conditions. One is between the specimen and the upper part of seesaw, and the other is between the main body and the lower part of seesaw. The contact conditions in the model are assumed to have surface-to-surface contact with a friction coefficient of $\mu = 0.2$, and finite sliding is allowed. The bottom of the mount is fixed. A displacement-controlled boundary condition is applied at the upper surface of the jig where it is connected to the loading rod of the main frame of the test machine (the screw hole shown in Fig. 2 is not modeled). The misalignments considered in Fig. 3 are implemented by moving or rotating the elements of plates, adhesive, and mount.

The boundary conditions of the seesaw are complicated because the seesaw is free and naturally lays on the main body in the gravitational field and its initial position is undetermined before loading. In order to simplify the motion of the seesaw, we apply equivalent forces at the inside of the groove. We assume that the center of mass of the seesaw is inside the groove, and it is enforced to stay in the concave space of the groove. Therefore, unexpected excessive rotation of the seesaw is prevented. As a result, downward equivalent forces (weight is 0.23 grams) corresponding to the gravitational force, are applied to the upper third nodes over the central contact line between the seesaw and main body.

The material properties are listed in Table 1. The jig and seesaw are made of steel. The upper and lower plate are made of silicon and covered with a film adhesive layer. The mounting block for specimen attachment is made of aluminum.

Table 1. Material properties of applied materials.

Material	Young's modulus (GPa)	Poisson's ratio
Steel jig	207.0	0.33
Aluminum base	72.0	0.33
Epoxy adhesive	5.0	0.34
Silicon	130.0	0.3
Film adhesive	3.0	0.35

3.2 Cohesive zone model for crack propagation

The debonding of the adhesive was modeled by using a CZM. There are several techniques to implement the CZM. In this study, a relatively simple technique is applied because the quantitative characteristics of delamination behavior depending on the structure of the jig is the scope of this study. The applied techniques are briefly summarized in this section.

Elastic behavior can be defined as

$$\mathbf{t} = E\varepsilon \tag{2}$$

where t is the nominal traction stress vector, E is the elastic stiffness, and ε is the strain. In this study, we specified E_{nn} = 20 GPa, E_{ss} = 10 GPa and E_{tt} = 10 GPa. The subscripts n, s and t represent the normal, first shear, and second shear direction, respectively.

For delamination, the traction separation law was applied. Damage was assumed to initiate when a quadratic interaction of a function involving the nominal strain ratios reaches a value of one. This criterion can be represented as

$$\left\{\frac{\langle \varepsilon_n \rangle}{\varepsilon_n^o}\right\}^2 + \left\{\frac{\varepsilon_s}{\varepsilon_s^o}\right\}^2 + \left\{\frac{\varepsilon_t}{\varepsilon_t^o}\right\}^2 = 1 \tag{3}$$

where the superscript 0 represents the peak value of nominal strain. The symbol <> is a Macaulay bracket and denotes the positive part. In this study, all ε_n^0, ε_s^0 and ε_t^0 are set to be 0.1.

Damage evolution based on effective displacement was applied. For linear softening, we used an evolution of damage variable, D [21] :

$$D = \frac{\delta_m^f \left(\delta_m^{\max} - \delta_m^0\right)}{\delta_m^{\max}\left(\delta_m^f - \delta_m^0\right)} \tag{4}$$

where $\delta_m^{\max}$ refers to the maximum value of the effective displacement attained during the loading history, δ_m^f is the effective displacement at complete failure, and δ_m^0 is the effective displacement at damage initiation. In this study, displacement at failure was assumed to be 1.0 μm. For simplicity, a mode-independent condition was assumed.

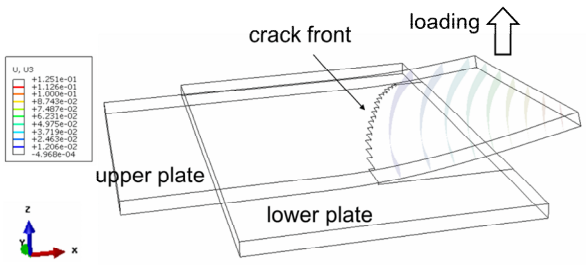

Fig. 6. Deformed shape of the rotation of 0.5 ° about x-axis when a fixed jig is applied.

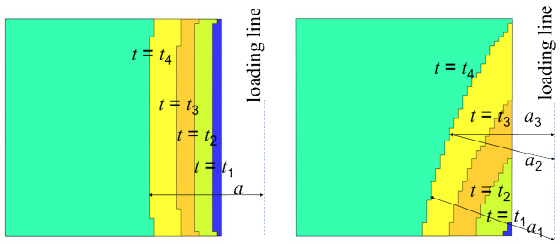

Fig. 7. Overlay plot of crack propagation by fixed jig (a) without rotation; (b) with rotation of 0.5°.

4. Results of analysis

Fig. 6 shows deformed shape of specimen when a fixed jig is used. There is an adhesive layer between lower plate and upper plate. Specimen is rotated about x-axis. Contours represents z directional displacement. For 3-dismensional view, transparency of the body is applied. It is clearly shown that there is a crack front by the removal of damaged element.

Crack fronts are shown in Figs. 7-10. Only the adhesion layer is drawn in the xy-plane for a clear view. The area of the adhesive is 9.5 x 9.5 mm^2. As a result of the external load, damage is accumulated in the adhesive. When it reaches full damage (the damage parameter equals 1.0), the element is removed. Therefore, the crack front can be identified by checking the exterior edges of the remaining elements.

Fig. 7(a) shows crack fronts over time if alignment is perfect (no misalignment). Four deformed shapes are overlaid. It is shown that the crack propagates from right to left sequentially with vertically well aligned crack fronts. Fig. 7(b) shows crack fronts over time when the fixed jig is used with a 0.5° rotation. Note that the time scales are not the same as Fig. 7(a). In the early stage ($t = t_1$), stress concentrates at the lower corner where the jig first makes contact with the specimen. Then, the crack begins to propagate and several meshes are removed. The crack then propagates gradually with slanting ($t = t_2 \sim t_4$). As shown in Fig. 7(a), the crack length 'a' can be clearly defined from loading line to crack front, where the loading line is contacting line between loading jig and upper plate. However, in Fig. 7(b), the crack length is not defined uniquely; a_1, a_2, or a_3. In this study, representative crack length is extracted from compliance and displacement relation in Ref. [15].

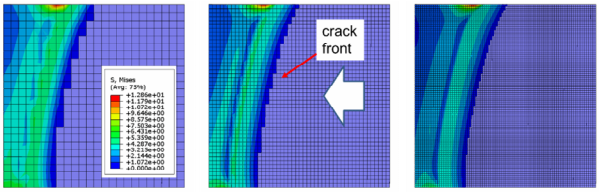

Fig. 8. Comparison of the effect of mesh size: (a) 0.4 x 0.4 mm^2; (b) 0.2 x 0.2 mm^2; (c) 0.1 x 0.1 mm^2.

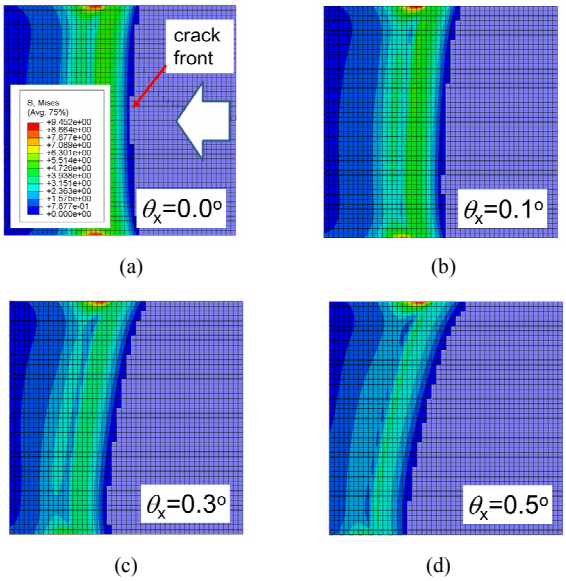

Fig. 9. Crack propagation of fixed jig with respect to the rotation angle about x-axis: (a) 0.0°; (b) 0.1°; (c) 0.3°; (d) 0.5°.

Fig. 8 shows the dependency of mesh size on the behavior of crack propagation. The evaluated mesh sizes in the xy-plane are (a) 0.4 x 0.4 mm^2, (b) 0.2 x 0.2 mm^2 and (c) 0.1 x 0.1 mm^2 (all of the z thicknesses are 0.01 mm). For visualization, both deformed and undeformed shapes are shown overlapped. The crack propagates from the right to the left. As shown in these figures, overall shapes of the crack fronts look similar, independent of mesh size. Therefore, our reference mesh size was chosen as type (b): 0.2 x 0.2 mm^2, because type (a) was too coarse and type (c) required to much computational time.

Characteristics of crack propagation for the two types of jigs are compared in Figs. 9 and 10. Crack fronts of the fixed jig are shown in Fig. 9 as a function of the degree of rotational misalignment. When the specimen is well positioned (Fig. 9(a), rotation of 0°), it shows vertically straight propagation. However, as shown in Fig. 9(b), even a small rotation of 0.1° makes the crack slant. The slant becomes larger with increasing rotation angle. When it reaches a rotation of 0.5°, the slant angle of the crack front becomes very large.

When the rotatable jig designed in this study is applied, crack fronts are shown in Fig. 10. It is observed that there is no asymmetric mesh up to rotation of 0.5° (Fig. 10(a)). When

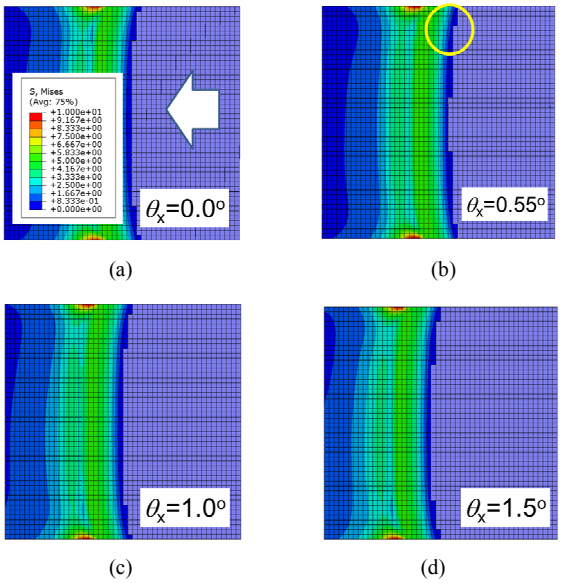

Fig. 10. Crack propagation of rotatable jig with respect to the rotation angle about x-axis: (a) 0°; (b) 0.55°; (c) 1.0°; (d) 1.5°.

the angle becomes 0.55°, first one asymmetric mesh appears as shown in Fig. 10(b). Even the rotation angle of 1.5°, it keeps overall symmetrical shape of crack front.

The effect of rotation about x-axis is parameterized by counting the number of asymmetric meshes. Note that the number of asymmetric meshes depends on the mesh size, so it is a qualitative parameter. The number of asymmetric meshes is plotted in Fig. 11 as a function of rotation angle with blanked square symbol. One asymmetric mesh appears at 0.55°. At the angle of 2.0°, seven asymmetric meshes appear. In general, the asymmetry increases with rotation angle. Nevertheless, the asymmetry is sufficiently reduced compared to the fixed jig. The results of the fixed jig are not plotted because just a small rotation produces asymmetric crack propagation, as shown in Fig. 9.

The energy release rate is calculated by Eq. (1). Critical load P_c is extracted from the reaction force of upward jig movement of 0.05 mm. Compliance is calculated from the reaction force and jig movement. Crack length is extracted from the relation between the compliance and beam deflection [15]. There were no distinctive differences in crack lengths for each case. Right y-axis in the Fig. 11 represents percent deviation of energy release rate compared with the reference G of 2.90 mJ/mm^2 without misalignment. It is shown that the deviation of G increases with increasing rotational angle. However, the deviation is less than 1.0 % up to the rotation of 2.0°.

Fig. 11(b) shows the deviation of G of fixed jig and rotatable jig. The deviation of G of fixed jig increases exponentially with increasing rotational misalignment even smaller than 0.5°. As a result, it is clearly shown that the rotatable jig dramatically decreases the effect of rotational misalignment and keeps the deviation under 1.0 %. Note that the rotation of the specimen could be controlled less than 1.0°, experimentally.

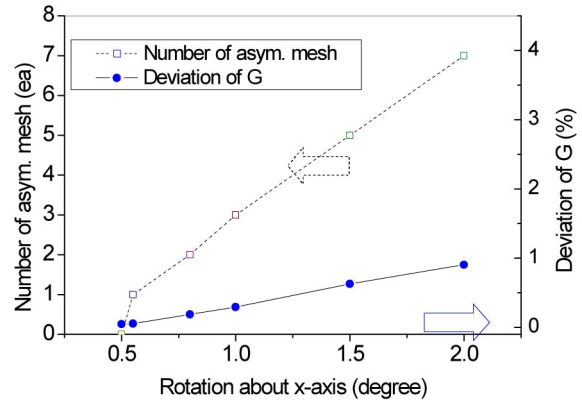

(a)

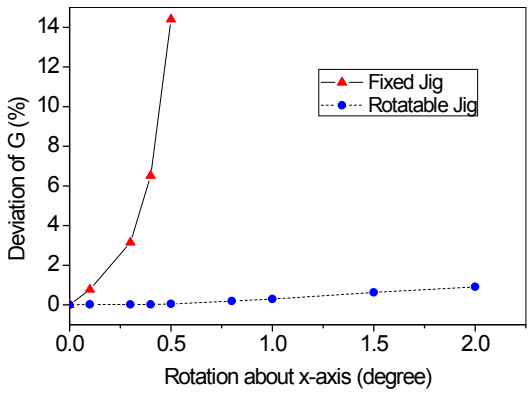

(b)

Fig. 11. (a) Number of asymmetric meshes and deviation of energy release rates as a function of the rotational misalignment about x-axis; (b) deviation of energy release rate fixed jig and rotatable jig.

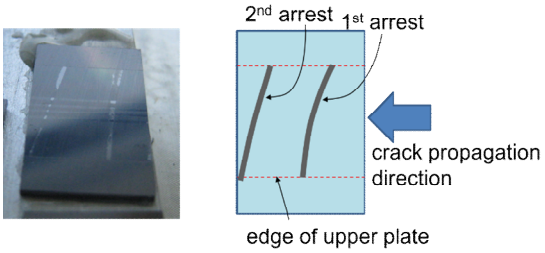

(a) (b)

Fig. 12. (a) Photograph of surface of delaminated bottom plate of fixed jig; (b) schematics of the surface in xy-plane.

Fig. 12(a) shows the experimental results of a crack front obtained by a slightly rotated jig [15]. The figure shows a detached surface of the lower plate after the test. The delamination occurred from right to left. The two white-colored lines show crack arrested locations during crack propagation. Fig. 12(b) shows a schematic of the surface with two slanted lines. It is shown that the FEA results well agree with experimental results.

Fig. 13 shows a photograph and schematic of the delamination surface obtained by the rotatable jig. Although it is not

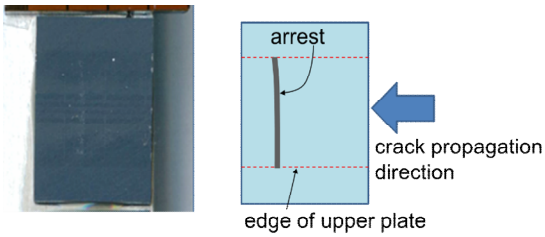

(a) (b)

Fig. 13. (a) Photograph of surface of delaminated bottom plate of rotatable jig; (b) schematics of the surface in xy-plane.

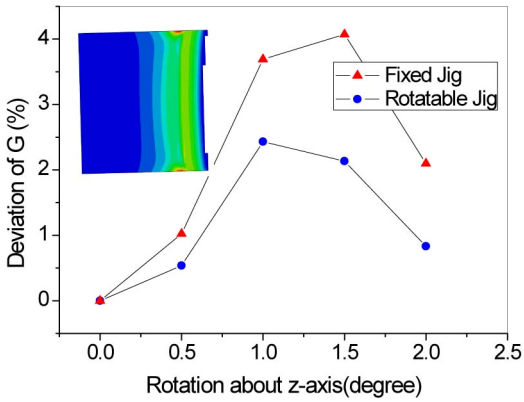

Fig. 14. Deviation of energy release rate as a function of the rotation misalignment about z-axis.

clearly shown in the photo, there is a light white-colored line around the center of the specimen, and this is expressed in the schematic. The line is almost straight and vertical.

The effect of rotation about z-axis is shown in Fig. 14. Deviation of G is calculated by similar way with Fig. 11. It is shown that the deviation increases with increasing rotational angle. Geometrically, the rotational misalignment makes the same amount of rotation of crack front. For example, rotational angle of 1.2° makes slanting distance of 0.2 mm (= 9.6 mm × tan(1.2°)) which is the same as the size of a mesh. When the rotation about z-axis is greater than 1.5°, the deviation of G looks decreasing. It is found out that the decreasing is resulted from the change of shape of cantilever from rectangular to parallelogram, which reduces the apparent stiffness of cantilever beam. That is to say, the reduction of deviation is not related to the adhesion of adhesive but the shape of cantilever. In spite that the deviation of G of rotatable jig shows less deviation than the fixed jig, the rotatable jig is insufficient to overcome the z-axis rotational misalignment. However, experimentally, the rotational angle can be easily controlled within 0.5° if the experiment is carefully performed. An inset in the figure is crack front of the adhesive layer of rotatable jig under the rotation of 1.5° about z-axis.

Another uncertain factor of the seesaw system is the effect of displacement misalignment in the y-direction. Fig. 15 shows the deviation of G as a function of misalignment in the y-direction. It is shown that the fixed jig is not affected by the

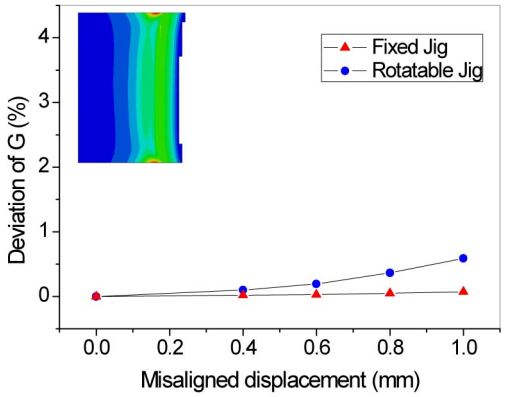

Fig. 15. Deviation of energy release rate as a function of misaligned displacement in y-direction.

y directional displacement. Rotatable jig shows slight increase of deviation as a function of translational misalignment. It is due to the fact that the loading position (seesaw groove) changes by the same amount as the translational misalignment based on the center of specimen. However, the magnitudes of the deviation of G are less than 0.6 % up to the displacement of 1.0 mm. Experimentally, a misalignment larger than about 0.5 mm can be easily noticed with the naked eye and hence can be adjusted during the test process. Therefore, it is thought that the y-directional deviation can be controlled if the experiment is performed carefully. An inset in the figure is crack front of the adhesive layer of rotatable jig under the translation of 0.8 mm in y-axis.

5. Conclusions

The performance of jig was verified by finite element analysis. Following three critical misalignments were considered.

(1) Rotational misalignment about x-axis:

The fixed jig showed severe distortion of the crack propagation shape. Even a small rotation about 0.1 ^{o} made the crack slant. The slant becomes larger with increasing rotation angle. The deviation of G of fixed jig increases exponentially with increasing rotational misalignment even smaller than 0.5 ^{o}.

The rotatable jig showed almost perfect symmetric crack front up to a rotation angle of 0.5^{o}, and showed symmetric shape regardless of rotation. The rotatable jig dramatically decreases the effect of rotational misalignment and keeps the deviation of G under 1.0 %.

(2) Rotational misalignment about z-axis:

The deviation of G of fixed jig and rotatable jig increased with increasing rotational misalignment about z-axis. The rotatable jig showed less deviation than the fixed jig. The rotational movement of seesaw slightly compensated the misalignment. Excessive rotation of specimen made the cantilever of SCB from rectangular shape to parallelogram shape, which reduces the apparent stiffness of cantilever beam.

(3) Translational misalignment in y-axis:

The fixed jig was not affected by the y directional displacement. However, the rotatable jig showed small increasing of deviation as a function of translational misalignment. However, the magnitudes of the deviation of G were less than 0.6 % up to the displacement of 1.0 mm.

In conclusion, the fixed jig was not appropriate for single cantilever beam test method when the length of the cantilever was relatively short, because the jig showed large deviation of energy release rate by the small rotational misalignment of specimen about x-axis. However, the rotatable jig was appropriate for the measurement of adhesion of small specimen, because the shape of the crack front remained almost symmetric shape and small deviation of energy release rate within the range of common misalignment.

Acknowledgment

(1) This work was supported by the 2014 Yeungnam University Research Grant.

(2) This research was supported by Basic Science Research Program through the National Research Foundation of Korea (NRF) funded by the Ministry of Education (NRF-2015R1D1A1A01061205).

References

[1] S. Takeda and T. Masuko, Die attach adhesives and films, *Materials for advanced packaging*, Springer Science Business Media (2009).

[2] X. Gagnarda and T. Mourierb, Through silicon via: From the CMOS imager sensor wafer level package to the 3D integration, *Microelectronic Engineering*, 87 (3) (2010) 470-476.

[3] V. K. Khanna, Adhesion-delamination phenomena at the surfaces and interfaces in microelectronics and MEMS structures and packaged devices, *J. of Physics D: Applied Physics*, 44 (3) (2011) 034004 (19).

[4] H. Shi and T. Ueda, Comparative studies on solder joint reliability of CTBGA assemblies with various adhesives using the array-based package shear test, *Microelectronics Reliability*, 51 (9-11) (2011) 1898-1902.

[5] *MIL-STD-883J*, Method 2019.7, Test Method Standard, Microcircuits.

[6] D. K. Shin, Y. H. Song and J. Im, Effect of PCB surface modifications on the EMC-to-PCB adhesion in electronic packages, *IEEE Tr. on Components and Packaging Technology*, 33 (2) (2010) 498-508.

[7] X. S. Dai, M. V. Brillhart and P. S.Ho, Adhesion measurement for electronic packaging applications using double cantilever beam method, *IEEE Tr. on Components and Packaging Technology*, 23 (2000) 101-116.

[8] M. F. Kanninen, An augmented double cantilever beam

model for studying crack propagation and arrest, *Int. J. Fract*., 9 (1973) 83-92.

[9] L. A. Carlsson and G. A. Kardomateas, Analysis of debond fracture specimens, *Structural and Failure Mechanics of Sandwich Composites*, Springer, Netherlands (2011).

[10] J. G. Ratcliffe and J. R. Reeder Jr., Sizing a single cantilever beam specimen for characterizing facesheet-core debonding in sandwich structure, *Journal of Composite Materials,* 45 (2011) 2669-2684.

[11] M. Rinker, M. John, P. C. Zahlen and R. Schäuble, Face sheet debonding in CFRP/PMI sandwich structures under quasi-static and fatigue loading considering residual thermal stress, *Engineering Fracture Mechanics,* 78 (2011) 2835-2847.

[12] J. Jumel, S. Chauffaille, M. K. Budzik, M. E. R. Shanahan and J. Guitard, Viscoelastic foundation analysis of single cantilevered beam (SCB) test under stationary loading, *European Journal of Mechanics - A/Solids,* 39 (2013) 170-179.

[13] S. Chauffaille, J. Jumel and M. E. R. Shanahan, Pre-cracking behaviour in the single cantilever beam adhesion test, *I. J. of Fracture,* 169 (2) (2011) 133-144.

[14] Z. Chen, B. Cotterell and W. T. Chen, Characterizing the interfacial fracture toughness for microelectronic packaging, *Surface and Interface Analysis,* 28 (1999) 146-149.

[15] D. K. Shin, J. J. Lee, C. K. Yoon, G. J. Lee, J. K. Hong and N. S. Kim, Development of single cantilever beam method to measure the adhesion of thin film adhesive on silicon chip, *Engineering Fracture Mechanics,* 133 (2015) 179-190.

[16] P. F. Liu and J. Y. Zheng, Recent developments on damage modeling and finite element analysis for composite laminates: A review, *Materials and Design,* 31 (2010) 3825-3834.

[17] D. K. Shin and J. J. Lee, Numerical analysis of dynamic T stress of moving interfacial crack, *I. J. of Fracture,* 119 (3) (2003) 223-245.

[18] R. D. S. G. Campilho, M. D. Banea, J. A. B. P. Neto and L. F. M. da Silva LFM, Modelling adhesive joints with cohesive zone models: effect of the cohesive law shape of the adhesive layer, *I. J. of Adhesion and Adhesives,* 44 (2013) 48-56.

[19] M. Rinker, M. John, P.C. Zahlen and R. Schäuble, Face sheet debonding in CFRP/PMI sandwich structures under quasi-static and fatigue loading considering residual thermal stress, *Engineering Fracture Mechanics,* 78 (2011) 2835-2847.

[20] H. J. Bang, S. K. Lee, C. D. Cho and J. U. Cho, Study on crack propagation of adhesively bonded DCB for aluminum foam using energy release rate, *J. of Mechanical Science and Technology*, 29 (1) (2015) 45-50.

[21] P. P. Camanho and C. G. Davila, Mixed-mode decohesion finite elements for the simulation of delamination in composite materials, *NASA/TM-2002-211737* (2002) 1-37.

Dong-Kil Shin is a Professor of School of Mechanical Engineering at Yeungnam University. He received the B.S. degree in mechanical engineering from Yonsei University, Korea, and the M.S. and Ph.D. degrees in mechanical engineering from the KAIST, Korea. His current research interests include the analysis of failure mechanism, reliability of electronic packaging and smart sensors.